Proceedings of 20th International Congress on Acoustics, ICA 2010

23-27 August 2010, Sydney, Australia

The physics of wedge diffraction: high-frequency approximate solution in the vicinity of shadow boundary

Mitsuhiro UEDA

Predio Meguro Science Laboratory, 4-20-13 Meguro, Meguro-ku, Tokyo, Japan

PACS: 43.20.EI

A top-down physical principle called virtual discontinuity principle of diffraction is proposed by us for analyzing waves diffracted by perfectly reflecting objects and a mathematical model is formulated to calculate diffracted waves by a sum of two elementary diffracted waves. The model is applied to waves diffracted by a wedge and high-frequency approximate solution for diffracted waves is deducted from the model that works at any angle of observation point. In the conventional analysis the approximate solution is derived from the rigorous solution, but it does not work when the observation point lies in the vicinity of shadow boundary. The success in our model is due to the simple structure introduced by the elementary diffracted waves. Thus the principle is validated firmly by this result and the implication of the new principle is discussed shortly.

1. INTRODUCTION

We have proposed a new physical principle that is called virtual discontinuity principle of diffraction for analyzing waves diffracted by perfectly reflecting objects and formulated a mathematical model for calculating diffracted waves by a sum of two elementary diffracted waves [1],[2]. The special merit of our model lies in the fact that diffracted waves calculated by the model always satisfies the boundary condition at the surface of the object This property is not supported by other principles for analyzing diffracted waves, for examples, Kirchhoff's formula [3], geometrical theory of diffraction [4], and Boundary Element Method [5].

The model is applied to waves diffracted by a wedge and high-frequency approximate solution for diffracted waves is deducted from the model that is exactly the same as the one that has been already derived from the rigorous solution of waves diffracted by the wedge [2]. It is rare to find the relation derived from the rigorous solution in the relations deducted from the model formulated by a top-down physical principle. Thus the principle is validated fairly by this result. The above approximate solutions, however, do not work in the vicinity of shadow boundary. The role of diffracted waves lies in the compensation of discontinuity caused by the geometrical optics solution, that is, discontinuity at shadow boundary. Thus the above agreement may not be enough to validate the principle firmly.

In this presentation high-frequency approximate solution that works in the vicinity of shadow boundary is deducted from the model, whereas it is not succeeded in deriving this relation from the rigorous solution since shadow boundary in diffracted waves occurs at two angles and that angles change complicatedly as a function of wedge and source angles. On the other hand shadow boundary in elementary diffracted waves occurs at one angle and it equals to the source angle. This outstanding simplification enabled by the new model makes it possible to deduct the high-frequency approximate solution near shadow boundary from the model and it is combined with the conventional one so that the approximate solution can be applied at any angle of observation. The accuracy of the approximate solution is examined by comparing it with the rigorous solution and that of the new approximate solution in the vicinity of shadow boundary is almost the same as that of the conventional one at far outside of shadow boundary. This would validate the new principle further since it should make the analysis remarkably simpler.

This paper is organized as follows. In Sec.2 wedge-shaped region and potential in the region are mathematically defined. In Sec.3 a virtual space is formulated by incorporating mirror images reflected by edges of wedge. In Sec.4 the Green's theorem is applied to the virtual space to formulate a mathematical model for diffracted waves in terms of elementary diffracted waves. In Sec.5 some properties of diffracted waves are derived from the model. In Sec.6 high-frequency approximate solution of elementary diffracted waves is deducted from the model using potentials in free space and nondiffractive wedges. These potentials are useless in the conventional analysis since no diffracted waves are existed in them but elementary diffracted waves can exist in them. In Sec.7 high-frequency approximate solution of diffracted waves is calculated by the model and compared with the rigorous solution. A short summary and discussion on the implication of the new principle are given in Sec.8.

2. PRELIMINARIES

2.1 Wedge-shaped region

Draw a half line in the two-dimensional space and denote the starting point as Q and introduce the polar coordinate system $\boldsymbol{r} = (r, \theta)$ by specifying r as a distance measured from Q and θ as an angle measured from the half line in the anti-clockwise direction. Let W_0 be a wedge-shaped region (abbreviated by wedge) of apex angle 2Φ and be defined by

$$W_0 = \{(r, \theta) \,|\, r \geq 0, -\Phi \leq \theta \leq \Phi\} \qquad (1)$$

where $0 < \Phi \le \pi$ and $\Phi = \pi$ corresponds to an semi-infinite plane, $\Phi > \pi/2$ a concave wedge, $\Phi < \pi/2$ a convex wedge and $\Phi = \pi/2$ a reflecting plane. The apex of W_0 lies on Q and W_0 is bounded by two edges B_0^a and B_0^c. Let $L(\theta)$ denote an half line that starts from Q and runs in the θ direction. Then the edges can be specified as $B_0^a = L(\Phi)$ and $B_0^c = L(-\Phi)$.

2.2 Potential

The waves propagating in W_0 are stationary in time and satisfy the following relation

$$\nabla^2 U + k^2 U = -\delta(\boldsymbol{r} - \boldsymbol{r_S}) \qquad (2)$$

where U stands for the potential of waves, $k = (2\pi/\lambda)$ the wave number (λ : the wavelength), δ the delta function, $\boldsymbol{r_S} = (r_S, \theta_S)$ the position vector of the point source S and the relations $0 < r_S < \infty$ and $-\Phi < \theta_S < \Phi$ hold. In the free space S radiates the direct waves U^F that is given by

$$U^F(\boldsymbol{r} \mid \boldsymbol{r_S}) = \mathrm{H}_0^{(2)}(k\,|\boldsymbol{r} - \boldsymbol{r_S}|)/(4j) \qquad (3)$$

where $\mathrm{H}_0^{(2)}$ stands for the 0-th order Hankel function of the second kind, j the imaginary unit and the stationary time function exp($j\omega t$) is deleted where ω stands for the angular frequency.

As to the boundary condition, the Dirichlet condition ($\partial U/\partial \boldsymbol{n}$=0) or the Neumann condition (U=0) is set to edges of the wedge where $\boldsymbol{n}$ stands for an inner unit vector normal to the edges. Let us denote the wedge that satisfies the Dirichet condition as the hard wedge and the Neumann condition as the soft wedge. The edge of the hard wedge can be regarded as a mirror of $m = 1$ where m stands for the reflection coefficient of the mirror. Similarly the edge of the soft wedge can be regarded as a mirror of $m = -1$. In this paper the distinction between the hard and soft wedges is made by the numerical value of m.

The diffracted waves can be considered as a deviation from the geometrical optics waves. Then the potential can be expressed as

$$U(\boldsymbol{r}) = U^G(\boldsymbol{r}) + U^D(\boldsymbol{r}) \qquad (4)$$

where U^G stands for the potential for the geometrical optics waves and U^D that for the diffracted waves.

2.3. Elementary diffracted waves

In this paper a new field quantity that is called elementary diffracted waves is introduced by the following relation

$$E(r,\theta) = \int_{L(\theta)} -g(k(r+\ell))\partial U(\boldsymbol{r}_\ell)/\partial \boldsymbol{n}_\ell \, d\ell \qquad (5)$$

where E stands for the potential for the elementary diffracted waves, ℓ the coordinate taken along $L(\theta)$, $\boldsymbol{r_\ell}$ the position vector of a point on $L(\theta)$, $\boldsymbol{n}_\ell$ an unit vector normal to $L(\theta)$ taken in the anticlockwise direction as shown in Figure 1, and g the Green's function that is given by

$$g(x) = \mathrm{H}_0^{(2)}(x)/(4j). \qquad (6)$$

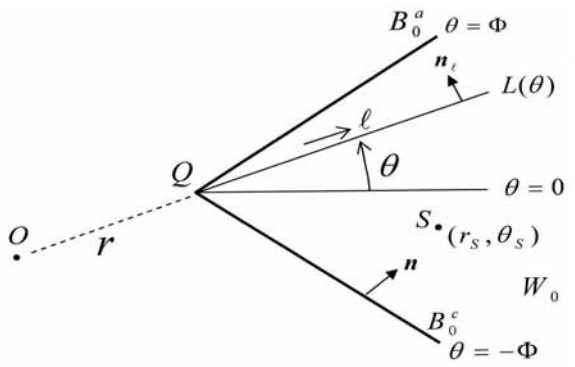

Figure 1 Calculation of elementary diffracted waves

Our model for wedge diffraction described in this paper is formulated in terms of E and it can be calculated using U in W_0 as seen in (5). Physically, however, E is considered as a contribution of U on $L(\theta)$ to the point O ,that is, located at $(r, \theta + \pi)$ as shown in Fig.1. But in this case O is not included in W_0. Inversely if O is kept in W_0, it might be necessary to draw $L(\theta)$ in the outside of W_0. Thus it is necessary to make the physical concept of E compatible to the structure of the space that is under consideration.

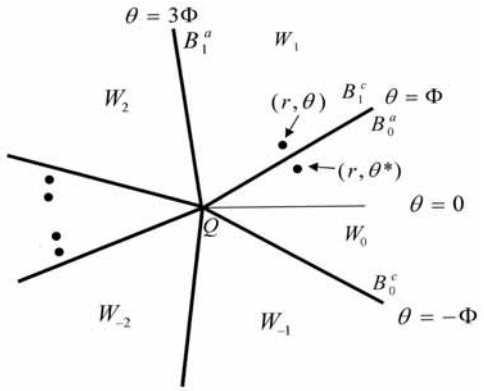

Figure 2 Extention of wedge-shaped region

3. FORMATION OF A VIRTUAL SPACE

3.1 Extension of a wedge-shaped region

Extend the wedge-shaped region beyond the edges by considering the edges B_0^a and B_0^c as mirrors and mirrored images are assumed to be spread out beyond the edges. The wedges $W_i, i = 1,2,3,...$ are spread out beyond B_0^a and the wedges $W_i, i = -1,-2,-3,...$ are spread out beyond B_0^c where i stands for a number of wedge and $|i|$ corresponds to the reflection number. The wedge W_i is bounded by $L((2i+1)\Phi)$ and $L((2i-1)\Phi)$ and let us denote the former as B_i^a and the latter as B_i^c. If a point in W_0 that is specified by (r, θ^*) is imaged to a point (r, θ) in W_i by mirror reflections as shown in Figure 2, then the following relations

$$i = w(\theta) = \mathrm{int}(\theta/2\Phi + \mathrm{sgn}(\theta)/2) \qquad (7)$$

$$\theta^* = (-1)^i(\theta - 2i\Phi) \qquad (8)$$

$$\theta = (-1)^i\theta^* + 2i\Phi \qquad (9)$$

hold where $w(\theta)$ stands for the number of wedge in which $L(\theta)$ runs , $\mathrm{int}(x)$ the integral part of the real number x , and $\mathrm{sgn}(x)$ the sign of x that is equal to $x/|x|$ for $x \neq 0$ and 0

for $x = 0$. Let us denote θ^* as the original angle of θ. Then the potential at (r, θ) can be assigned by the following relation

$$U(r,\theta) = m^i U(r,\theta^*) \tag{10}$$

where i and θ^* are calculated by (7) and (8) and m^i reflects the amplitude reversal in case of the soft wedge ($m = -1$). Since the original angle is symmetric with respect to the edge, U in the hard wedge is symmetric with respect to the edge and antisymmetric in the soft wedge. According to the boundary conditions, that is, $\partial U/\partial\theta$=0 for the hard wedge and U=0 for the soft wedge, the continuity of U and $\partial U/\partial\theta$ at the edge holds for hard and soft wedges. Similarly the following relation holds for the elementally diffracted waves

$$E(r,\theta) = (-m)^i E(r,\theta^*). \tag{11}$$

Consequently $E(r,\theta)$ in the hard wedge is antisymmetric with respect to the edge and symmetric in the soft wedge. The continuity of E and $\partial E/\partial\theta$ at the edge also holds for hard and soft wedges since $E = 0$ is immediately obtained from (5) at the edge of the hard wedge and $\partial E/\partial\theta = 0$ can be also derived at that of the soft wedge. Thus U and E are extended beyond the edges continuously up to the 1st derivative.For the sake of later references, let S_i denote the mirror image of S in W_i and $\boldsymbol{r}_S(i) = (r_S, \theta_S(i))$ its position vector , then

$$\theta_S(i) = (-1)^i \theta_S + 2i\Phi \tag{12}$$

holds and the direct waves from S_i is expressed as

$$U_i^F(r,\theta) = m^i U^F(r,\theta \mid S = S_i) \tag{13}$$

where U^F in the right side is given by (3) if $\boldsymbol{r}_S$ is replaced by $\boldsymbol{r}_S(i)$.

3.2 Virtual space V

A virtual space V is defined as a space that can be observed by the observation point O that is placed at $\boldsymbol{r} = (r,\theta)$ in W_0 where mirror images are assumed to be spread out beyond the edges. Let us introduce a half line $D = L(\theta + \pi)$, that is, a half line that starts from Q and runs in the direction of $\theta + \pi$ as shown in Figure 3. It is also a half line to calculate $E(r,\theta+\pi)$ in (5). If a point on $L(\theta)$ is rotated in the anticlockwise direction until it touches D in W_p where $p = w(\theta + \pi)$ is a nonnegative integer. Let D^a express D that is running in W_p and W_p^D a truncated wedge that is bounded by B_p^c and D^a. Similarly if a point on $L(\theta)$ is rotated in the clockwise direction, it touches D in W_n where $n = w(\theta - \pi)$ is a nonpositive integer. Let D^c express D that is running in W_n and W_n^D a truncated wedge that is bounded by B_n^a and D^c. Then the virtual space V is formulated by

$$V = W_p^D \cup W_n^D \cup (\textstyle\sum_{i=n+1}^{p-1} \cup W_i). \tag{14}$$

If either $p = 0$ or $n = 0$ holds, the third term in the right side of (14) becomes zero. The potential on D^a and D^c are different for most cases and the potential in V is not continuous at D. Accordingly it is called as a virtual discontinuity line.

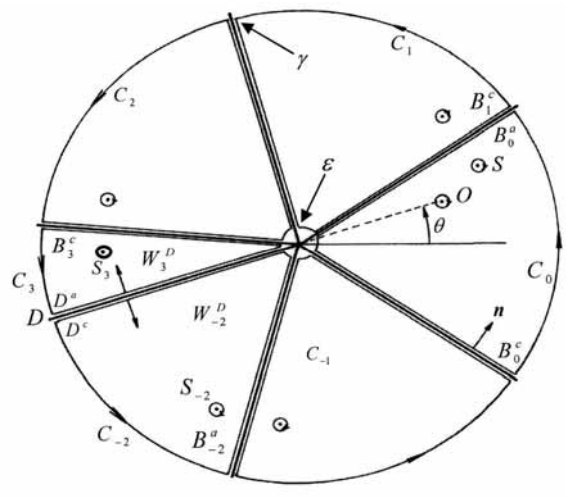

Figure 3 Formation of a virtural space

4. MODEL IN ELEMENTARY DIFFRACTED WAVES

Draw closed curves $C_i\ (i = n,..,0,..,p)$ in $W_n^D, W_i\ (i = n+1,..,0,..,p-1), W_p^D$ that comprise V as shown in (14). Each C_i is composed by two circular arcs of radius $\varepsilon\ (\varepsilon << 1)$ and $\gamma\ (\gamma >> 1)$ respectively and two segments connecting these arcs along the edges or D as shown in Figure 3. The centers of curvature of arcs lie on Q and the radii ε and γ are common for all C_i. Then the following relation is obtained by applying the Green's theorem to each C_i and taking a sum of the resulting relations

$$\sum_{i=n}^{p} \int_{C_i} U(\boldsymbol{r}_\ell)\partial g(k \mid \boldsymbol{r}_\ell - \boldsymbol{r} \mid)/\partial \boldsymbol{n} - g(k \mid \boldsymbol{r}_\ell - \boldsymbol{r} \mid)\partial U(\boldsymbol{r}_\ell)/\partial \boldsymbol{n}\, d\ell = 0 \tag{15}$$

where a circle of very small radius centered at O is included in C_0 and that centered at S_i in C_i. If S_n is not included inside C_n, no circle is added to C_n. The same story holds for S_p and C_p. As seen in Figure 3, two integral paths run parallel to the edge, that is, one in C_i and the other in C_{i+1} where $i = n,..., p-1$. Since the potential is continuous at edges, these pairs of integrals are cancelled out each other. And there remain the integrals along D^a and D^c since D is the only edge in Figure 3 where the potential is discontinuous. In this case O lies on the extension of D, then the following relations hold

$$| \boldsymbol{r}_\ell - \boldsymbol{r} | = \ell + r,\ \partial g/\partial \boldsymbol{n} = 0\,. \tag{16}$$

Thus at the limits of $\varepsilon \to 0$ and $\gamma \to \infty$, the integrals along D^a and D^c can be expressed by $-E(r,\theta+\pi)$ and $E(r,\theta-\pi)$ respectively and the integrals along the arcs become zeros. Consequently (15) can be rewritten as

$$\begin{aligned} U(r,\theta) &= (1/2 + \mathrm{sgn}(\theta + \pi - \theta_S(p))/2) U_p^F(r,\theta) \\ &+ (1/2 - \mathrm{sgn}(\theta - \pi - \theta_S(n))/2) U_n^F(r,\theta) \\ &+ \textstyle\sum_{i=n+1}^{p-1} U_i^F(r,\theta) \ - E(r,\theta+\pi) \ + E(r,\theta-\pi) \end{aligned} \tag{17}$$

where the direct waves are resulted from the integrals along the small circle centered at S_i and (13) is used. This is the expression of the potential of waves in the wedge in terms of the elementary diffracted waves. The first term in the right side of (17) takes U_p^F if S_p is included inside of W_p^D, $U_p^F/2$ if S_p is located on D^a, and 0 otherwise. And the same story holds for the second term of (17) since the sources S_p and S_n may not be included in the truncated wedges. In the third term S_i is always included in W_i so no sgn function is included in this term. The sum of the first three terms in (17) comprises the geometrical optics waves. Then as seen from (4) and (17) the potential for diffracted waves is expressed by the sum of the fourth and fifth terms in (17), that is,

$$U^D(r,\theta) = -E(r,\theta+\pi) + E(r,\theta-\pi) \tag{18}$$

and in terms of the original angles (18) is rewritten as

$$U^D(r,\theta) = -(-m)^p E(r,(\theta+\pi)^*) + (-m)^n E(r,(\theta-\pi)^*) \tag{19}$$

where $p = w(\theta+\pi)$ and $n = w(\theta-\pi)$. (18) and (19) correspond our model for diffracted waves in terms of elementary diffracted waves.

The physics of wedge diffraction is quite clear in (17) where the physics is illustrated in the virtual space. The first term in (17) changes discontinuously when D^a crosses S_p, that is, when the relation $\theta+\pi = \theta_S(p)$ holds, but this jump is compensated by the fourth term so that the potential changes continuously since $E(r,\theta)$ changes discontinuously at $\theta = \theta_S(i)$. The same story holds for the second term and in this case the jump occurs when $\theta-\pi = \theta_S(n)$ holds and it is compensated by the fifth term. On the other hand in the conventional analysis the physics must be illustrated in W_0. Let θ_{SB} be the angle at that U^D changes discontinuously and denote it as the angle for shadow boundary. Then as shown below in the section 5.3, θ_{SB} changes complicatedly as a function of θ_S and Φ. Accordingly the physics of wedge diffraction has been unclear in the convention theory of diffraction.

5. PROPERTIES OF DIFFRACTED WAVES

5.1 Boundary condition

Assume $\theta = -\Phi$ in (19), that is, calculate U^D at the boundary B_0^e. Then the following relations hold

$$p+n = -1,\ (-\Phi+\pi)^* = (-\Phi-\pi)^* \tag{20}$$

where (7) and (8) are used. Then inserting these relations into (19),

$$U^D(r,\theta)|_{\theta=-\Phi} = 0 \tag{21}$$

is resulted for the soft wedge $(m=-1)$ and

$$\partial U^D(r,\theta)/\partial\theta|_{\theta=-\Phi} = 0 \tag{22}$$

for the hard wedge $(m=1)$. The same story holds for U^D at the other boundary B_0^a. Consequently it becomes clear that the boundary conditions are satisfied in (18) and (19). It is the necessary condition that the expression for diffracted waves should satisfy but no conventional expressions have satisfied it so far.

5.2 Nondiffractive wedge

Let q be a natural number $(q = 1,2,...)$. Then the following relation holds

$$E(r,\theta) = E(r,\theta+4q\Phi), \tag{23}$$

since the original image is reconstructed after two consecutive mirror reflections. Then if

$$\Phi = \pi/2q \tag{24}$$

holds, the right side of (18) becomes zero, that is, $U^D \equiv 0$ holds for the soft and hard wedges. Let us denote the wedges that satisfy (24) as the nondiffractive wedges and q=1 corresponds to a reflecting plane and q=2 to a concave wedge of $\Phi = \pi/4$. This is the well-known result but in the conventional analysis of diffracted waves this fact is useless since there are no diffracted waves in these wedges. In this analysis, however, these wedges are very useful since E does exist in them and the potential in them can be expressed by the well-defined geometrical optics waves.

5.3 Angle for shadow boundary θ_{SB}

The potential $U^D(r,\theta)$ changes discontinuously at $\theta = \theta_{SB}$, $(-\Phi \le \theta_{SB} \le \Phi)$ as mentioned above. As seen from (18), this happens if either $\theta_{SB}+\pi$ or $\theta_{SB}-\pi$ is equal to $\theta_S(i)$ since $E(r,\theta)$ changes discontinuously at $\theta = \theta_S(i)$ where i stands for an integer. Assume the relation $\theta_{SB} = (\theta_S+\pi)^*$. Then the following relation is derived from (8)

$$\theta_{SB} - (-1)^p\pi = -(-1)^p 2p\Phi + (-1)^p\theta_S \tag{25}$$

where $p(=w(\theta_S+\pi))$ is a nonnegative integer. Thus if p is an odd integer, (25) is reduced to $\theta_{SB}+\pi = \theta_S(p)$ and if p is an even integer, it is reduced to $\theta_{SB}-\pi = \theta_S(-p)$. Thus the requirement for the shadow boundary is satisfied for any p. The same story holds for $\theta_{SB} = (\theta_S-\pi)^*$. Consequently the angle for the shadow boundary is given by

$$\theta_{SB} = (\theta_S \pm \pi)^* \tag{26}$$

where (7) and (8) are used to calculate the original angles in (26). Thus θ_{SB} changes complicatedly as a function of θ_S and Φ. This makes it difficult to analyze $U^D(r,\theta)$ in the vicinity of θ_{SB}. On the other hand the simple structure of the discontinuity points in $E(r,\theta)$ as mentioned above makes it simple and straight forward to analyze $E(r,\theta)$ in the vicinity of the discontinuity point.

6. HIGH-FREQUENCY APPROXIMATE SOLUTION

Calculate high-frequency approximate solution of $E(r,\theta)$ in the nondiffractive wedge firstly and then extend the result to the arbitrary wedge. The potential in the nondiffractive wedge is described by the geometrical optics solution and is given by

$$U(r,\theta\,|\,\Phi=\pi/2q)=\sum_{i=0}^{2q-1}m^iU^F(r,\theta\,|\,S=S_i) \qquad (27)$$

where (13) and (24) are used. Let $F(r,\theta)$ be the fundamental solution of $E(r,\theta)$ and is given by

$$F(r,\theta)=\int_{L(\theta)}-g(k(r+\ell))\partial\,\mathrm{H}_0^{(2)}(k\,|\,\boldsymbol{r}_\ell-\boldsymbol{r_S}\,|)/\partial\boldsymbol{n}/(4\,\mathrm{j})\,d\ell \qquad (28)$$

where (3) is used. As seen in (28), $F(r,\theta)$ corresponds to $E(r,\theta)$ in the free space, that is, there is the source S in the space but no scatterer and no diffracted waves in it. But as mentioned in the section 5.2, there are elementary diffracted waves in the space and the most fundamental characteristics of diffracted waves can be seen in them as shown below. Thus $F(r,\theta)$ is denoted as the fundamental solution. From (5), (27) and (28) $E(r,\theta)$ in the nondiffractive wedge is expressed as

$$E(r,\theta\,|\,\Phi=2\pi/q)=\sum_{i=0}^{2q-1}m^iF_i(r,\theta) \qquad (29)$$

where $F_i(r,\theta)$ is given by (28) if $\boldsymbol{r_S}$ is replaced by $\boldsymbol{r_S}(i)$.

In the analysis below, it is assumed that $kr, kr_S >> 1$, so the Hankel functions are approximated as

$$\begin{aligned}\mathrm{H}_0^{(2)}(x)&\cong(2/\pi x)^{1/2}\exp(-\mathrm{j}x+\mathrm{j}\pi/4),\\ \mathrm{H}_1^{(2)}(x)&\cong(2/\pi x)^{1/2}\exp(-\mathrm{j}x+\mathrm{j}3\pi/4).\end{aligned} \qquad (30)$$

6.1 High-frequency approximate solution of $F(r,\theta)$

Let us divide the space into two regions. One is a large angle region (abbreviated by *LR*) and is defined by the relation $|\theta-\theta_S|>\Omega$ where Ω is a constant that depends on kr and kr_S. The other is a small angle region (abbreviated by *SR*) and is defined by $|\theta-\theta_S|\le\Omega$. The relation (28) is evaluated for *LR* and *SR* separately.

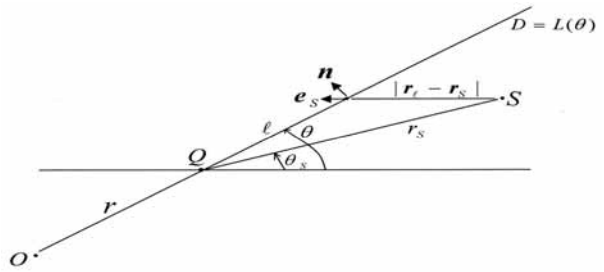

Figure 4 Analysis in large angle region *LR*

6.1.1 $F(r,\theta)$ in *LR*

The following relations hold in the vicinity of Q in Figure 4,

$$\partial H_0^{(2)}(k\,|\,\boldsymbol{r}_\ell-\boldsymbol{r_S}\,|)/\partial\boldsymbol{n}=-\mathrm{H}_1^{(2)}(k\,|\,\boldsymbol{r}_\ell-\boldsymbol{r_S}\,|)k\sin(\theta-\theta_S), \qquad (31)$$

$$|\,\boldsymbol{r}_\ell-\boldsymbol{r_S}\,|\cong r_S-\ell\cos(\theta-\theta_S). \qquad (32)$$

Then (28) can be rewritten as

$$F(r,\theta)=(\sin(\theta-\theta_S))\exp(-\mathrm{j}k(r+r_S)/(8\pi(rr_S)^{1/2})\int_0^\infty\exp(-\mathrm{j}k\ell(1-\cos(\theta-\theta_S)))\,d\ell, \qquad (33)$$

where (30) is used. Performing the integration by part and taking the first term, (33) can be rewritten as

$$F^{HL}(r,\theta)=R\cot((\theta-\theta_S)/2) \qquad (34)$$

where superscripts H and L stands for the high-frequency approximate solution and the large angle region respectively and R is a constant and is given by

$$R=-\mathrm{j}\exp(-\mathrm{j}k(r+r_S))/(8\pi k(rr_S)^{1/2}). \qquad (35)$$

As seen in (35), the amplitude of R is proportional to $1/(rr_S)^{1/2}$. Thus (34) shows the cylindrical waves from S that are scattered by the apex Q. Thus F^{HL} corresponds to the scattered component in F. As seen from (34), however, F^{HL} does not work in the vicinity of $\theta=\theta_S$.

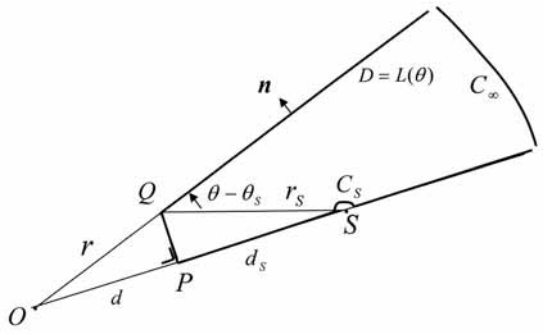

Figure 5 Analysis in small angle region SR

6.1.2 $F(r,\theta)$ in *SR*

Let P be a foot of perpendicular dropped from Q to the line OS and from a closed region connecting $L(\theta)$, PQ, a half line PS, a small half circle C_S that is centered at S, and a partial circle of very large radius C_∞ that is centered at Q as shown in Fig.5 and apply the Green's theorem to this closed region.. Then the following relation is obtained

$$-\mathrm{sgn}(\theta-\theta_S)U^F(r,\theta)/2+\int_{L(\theta)}-g\partial U^F/\partial n\,d\ell+\int_{QP}U^F\partial g/\partial n-g\partial U^F/\partial n\;d\ell=0. \qquad (36)$$

The contributions from PS and C_∞ are assumed 0 and the first term in the right side of (36) is the contribution from C_S and the second term corresponds to $F(r,\theta)$. Then (36) is rewritten as

$$F(r,\theta)=\mathrm{sgn}(\theta-\theta_S)U^F(r,\theta)/2-\int_0^a U^F\partial g/\partial n-g\partial U^F/\partial n\;d\ell \qquad (37)$$

where a stands for the length of PQ and is given by

$$a=\sin(\theta-\theta_S)rr_S/(d+d_S) \qquad (38)$$

where d and d_S stand for the length of OP and PS respectively. Thus the other expression of the fundamental solution is obtained. By assuming $|\theta-\theta_S|<<1$ and (30), (37) can be rewritten as

$$
\begin{aligned}
F^{HS}(r,\theta) &= \mathrm{sgn}(\theta-\theta_S)U^F(r,\theta)/2 \\
&\quad -\exp(-\mathrm{j}k(d+d_S))/(4\pi(dd_S)^{1/2}) \\
&\quad \cdot\int_0^a \exp(-\mathrm{j}k\ell^2(d^{-1}+d_S{}^{-1})/2)\,d\ell \\
&= \mathrm{sgn}(\theta-\theta_S)U^F(r,\theta)/2 \\
&\quad -\mathrm{Fr}(b)\exp(-\mathrm{j}k(d+d_S))/(4(\pi k(d+d_S))^{1/2})
\end{aligned}
\tag{39}
$$

where the superscript S stands for the small angle region and Fr the Fresnel function and is given by

$$
\mathrm{Fr}(x) = \int_0^x \exp(-\mathrm{j}\pi t^2/2)dt \tag{40}
$$

where $\mathrm{Fr}(-x) = -\mathrm{Fr}(x)$ and b is given by

$$
\begin{aligned}
b &= a(k(d^{-1}+d_S{}^{-1})/\pi)^{1/2} \\
&= \sin(\theta-\theta_S)krkr_S/(\pi kdkd_S(kd+kd_S))^{1/2}.
\end{aligned}
\tag{41}
$$

The second term of the right side of (39) becomes 0 at $\theta=\theta_S$ and the first term jumps from $-U^F/2$ to $U^F/2$. This jump is to compensate the discontinuity caused by the geometrical optics solution as mentioned in the section 4.

6.1.3 Role of Fresnel function

Let us study the role of the second term of the right side of (39). If the Fresnel function is approximated as follows

$$
\mathrm{Fr}(x) \cong (1-\mathrm{j})/2 + \exp(-\mathrm{j}\pi x^2/2)\{\mathrm{j}/(\pi x) - 1/(\pi^2 x^3)\} \tag{42}
$$

where $x>2$ is assumed, then the second term in (39) is rewritten as

$$
\begin{aligned}
&-\mathrm{Fr}(b)\exp(-\mathrm{j}k(d+d_S))/(4(\pi k(d+d_S))^{1/2}) \\
&= -\exp(-\mathrm{j}k(d+d_S))\{(1-\mathrm{j})/2\}/(4(\pi k(d+d_S))^{1/2}) \\
&\quad -\mathrm{j}\exp(-\mathrm{j}k(d+d_S)-\mathrm{j}\pi b^2/2+\mathrm{j}/\pi b^2)/(4\pi b(\pi k(d+d_S))^{1/2})
\end{aligned}
\tag{43}
$$

where $1+\mathrm{j}/\pi b^2 \cong \exp(\mathrm{j}/\pi b^2)$ is assumed. The first term of the right side of (43) corresponds to the high-frequency approximate expression of $-U^F(r,\theta)/2$. Thus this term is canceling the first term of the right side of (39) as b becomes larger than 2. The following relation is assumed to hold at $\theta-\theta_S=\Omega$

$$
-\mathrm{j}(kd+kd_S+\pi b^2/2-1/\pi b^2) = -\mathrm{j}(kr+kr_S). \tag{44}
$$

Then the second term of the right side of (43) can be rewritten as

$$
\begin{aligned}
&-\mathrm{j}\exp(-\mathrm{j}k(r+r_S))/(4\pi b(\pi k(d+d_S))^{1/2}) \\
&= -\mathrm{j}\exp(-\mathrm{j}k(r+r_S))/(\sin(\theta-\theta_S)4\pi k(rr_S)^{1/2}) \\
&= R(\cot((\theta-\theta_S)/2)+\tan((\theta-\theta_S)/2)) \\
&\cong F^{HL}(r,\theta)
\end{aligned}
\tag{45}
$$

where the identity $2/\sin x = \tan(x/2)+\cot(x/2)$ is used and $|\cot((\theta-\theta_S)/2)| >> |\tan((\theta-\theta_S)/2)|$ is assumed since $|\theta-\theta_S|$ is assumed to be very small. Consequently $F^{HS}(r,\theta)\cong F^{HL}(r,\theta)$ holds at $\theta-\theta_S=\Omega$ and the high-frequency approximate solution of $F(r,\theta)$ is given by

$$
F^H(r,\theta) = P_\Omega(\theta-\theta_S)F^{HS}(r,\theta) + (1-P_\Omega(\theta-\theta_S))F^{HL}(r,\theta) \tag{46}
$$

where $P_\Omega(x)$ takes 1 for $|x|\le\Omega$ and 0 otherwise. The relation (46) is the basic one in the analysis below.

As to the switching angle Ω, the following relations are obtained from (44)

$$
\pi b^2 \cong a_0, \tag{47}
$$

$$
a_0 = 2/(1/kr + 1/kr_S - 3/(kr+kr_S))^{1/3}. \tag{48}
$$

And from (38) and (41)

$$
\pi b^2 \cong a_1\sin^2(\theta-\theta_S) + a_1a_2\sin^4(\theta-\theta_S), \tag{49}
$$

$$
a_1 = (1/kr + 1/kr_S)^{-1},\ a_2 = (r^2+rr_S+r_S^2)/2(r+r_S)^2. \tag{50}
$$

Then from (47) - (50), Ω is expressed as

$$
\Omega \cong \sin^{-1}((a_0/a_1 - a_2(a_0/a_1)^2)^{1/2}). \tag{51}
$$

Note that three terms in $F^H(r,\theta)$, that is, $F^{HL}(r,\theta)$ and direct waves and Fresnel term in $F^{HS}(r,\theta)$, play their roles at right places. The direct waves in $F^{HS}(r,\theta)$ compensates the discontinuity caused by the geometrical optics solution at $\theta=\theta_S$ and the Fresnel term in $F^{HS}(r,\theta)$ is equal to 0 at this angle but it cancels the direct waves and introduces the scattered component so that $F^{HL}\cong F^{HS}$ holds at $|\theta-\theta_S|=\Omega$ and $F^{HL}(r,\theta)$ describes the scattered waves in *LR*. The Fresnel term plays the role to bridge the direct and scattered waves. This simple and straightforward structure of $F^H(r,\theta)$ deserves the name of the fundamental solution. The Fresnel function has been used in the analysis of diffraction frequently, but its role is made clear in this analysis. It is necessary, however, to insert the wedge in the space to release the elementary diffracted waves from the cancellation. In return $E(r,\theta)$ must satisfy the boundary condition at the edges of wedge.

6.2 High-frequency approximate solution of $E(r,\theta)$

By inserting (46) into (29), the high-frequency approximate solution of $E(r,\theta\,|\,\Phi=\pi/2q)$ is expressed as

$$
\begin{aligned}
&E^H(r,\theta\,|\,\Phi=\pi/2q) \\
&= \sum_{i=w(\theta-\Omega)}^{w(\theta+\Omega)} m^i(F_i^{HS}(r,\theta)-F_i^{HL}(r,\theta))P_\Omega(\theta-\theta_S(i)) \\
&\quad +\sum_{i=0}^{2q-1} m^iF_i^{HL}(r,\theta)
\end{aligned}
\tag{52}
$$

where $F_i^{HL}(r,\theta)$ and $F_i^{HS}(r,\theta)$ stand for $F^{HL}(r,\theta)$ and $F^{HS}(r,\theta)$ for $S=S_i$ respectively. The first term of the right side of (52) shows that the sources in *SR* must be included in $W_i, (i=w(\theta-\Omega),...,w(\theta+\Omega))$ where (7) is used. If the following identity is used [6]

$$
\sum_{i=0}^{q-1}\cot(-i\pi/q+x) = q\cot qx \tag{53}
$$

the second term in (52) can be reduced as

$$\sum_{i=0}^{2q-1} m^i F_i^{HL} E(r,\theta) = (\pi R/2\Phi)(\cot(\pi(\theta-\theta_S)/4\Phi) - m\tan(\pi(\theta+\theta_S)/4\Phi)). \quad (54)$$

The right side of (54) for the hard wedge $(m=1)$ becomes

$$(\pi R/\Phi)\cos(\pi\theta/2\Phi)/(\sin(\pi\theta/2\Phi)-\sin(\pi\theta_S/2\Phi)) \quad (55)$$

and is equal to zero at the boundary $\theta=(2i\pm1)\Phi$ where i stands for an integer. For the soft wedge $(m=-1)$ it becomes

$$(\pi R/\Phi)\cos(\pi\theta_S/2\Phi)/(\sin(\pi\theta/2\Phi)-\sin(\pi\theta_S/2\Phi)) \quad (56)$$

and its derivative is equal to zero at the boundary. Thus The right side of (54) satisfies the boundary conditions for an arbitrary wedge although the nondiffractive wedge is assumed in its derivation. Note that the first term of the right side of (52) takes non-zero values only in the vicinity of the source and the behavior of the potential near the source is almost the same for arbitrary wedge. Consequently the high-frequency approximate solution of $E(r,\theta)$ can be expressed as

$$E^H(r,\theta) = \sum_{i=w(\theta-\Omega)}^{w(\theta+\Omega)} m^i (F_i^{HS}(r,\theta) - F_i^{HL}(r,\theta)) P_\Omega(\theta-\theta_S(i)) + (\pi R/2\Phi)(\cot(\pi(\theta-\theta_S)/4\Phi) - m\tan(\pi(\theta+\theta_S)/4\Phi)) \quad (57)$$

As seen in (57), the direct and scattered waves that are contained in $E^H(r,\theta)$, are not separated in space, while those in $F^H(r,\theta)$, are separated. This may be considered as the expenditure to fulfill the boundary condition.

7. CALCULATION OF DIFFRACTED WAVES

From (18) and (57), the high-frequency approximate solution of $U^D(r,\theta)$ is expressed as

$$U^{DH}(r,\theta) = -E^H(r,\theta+\pi) + E^H(r,\theta-\pi) \quad . \quad (58)$$

If $|(\theta_S+\pi)*-\theta| > \Omega$ and $|(\theta_S-\pi)*-\theta| > \Omega$ hold, that is, if the observation point is placed far from the shadow boundaries, $E^H(r,\theta)$ is expressed by the second term of the right side of (57). Then after some algebraic calculation, (58) can be expressed as

$$U^{DH}(r,\theta) = z(\theta-\theta_S) + mz(\theta+\theta_S+2\Phi) \, , \quad (59)$$

$$z(x) = (\pi R/2\Phi)\{-\cot(\pi x/4\Phi + \pi^2/4\Phi) + \cot(\pi x/4\Phi - \pi^2/4\Phi)\} \, . \quad (60)$$

The relations (59) and (60) correspond to the conventional high-frequency approximate solution literally that is derived from the rigorous solution of waves diffracted by the wedge [7]. It is rare to find the relation derived from the rigorous solution in the relations deducted from the model formulated by a top-down physical principle. Thus the principle is validated fairly by this result. The above approximate solutions, however, do not work in the vicinity of shadow boundary. The role of diffracted waves lies in the compensation of discontinuity caused by the geometrical optics solution, that is, discontinuity at shadow boundary. Thus the above agreement may not be enough to validate the principle firmly.

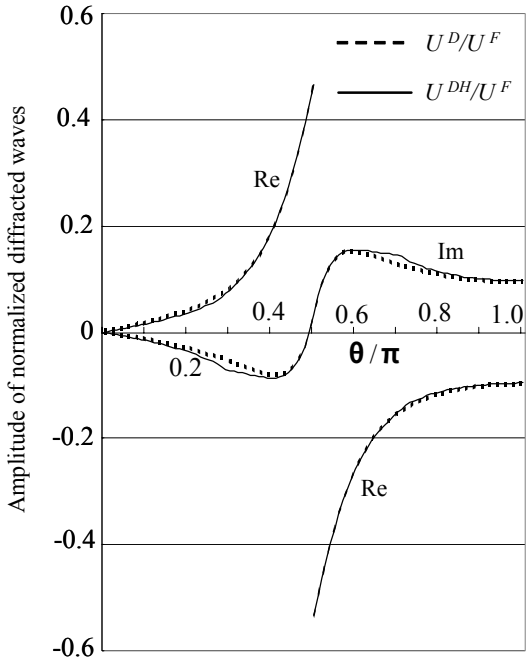

Figure 6 Comparison of approximate solution (58) and rigorous solution (61) for $\Phi=\pi$, $m=1$, $r=5\lambda$, $r_S=6\lambda$ and $\theta_S=0.5\pi$.

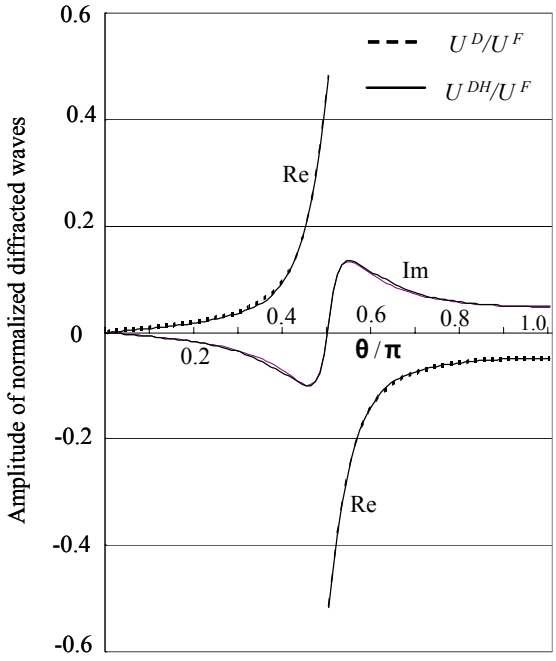

Figure 7 Comparison of approximate solution (58) and rigorous solution (61) for $\Phi=\pi$, $m=1$, $r=20\lambda$, $r_S=24\lambda$ and $\theta_S=0.5\pi$.

Since no high-frequency approximate solution that works in the vicinity of the shadow boundary, is derived from the rigorous solution, $U^{DH}(r,\theta)$ calculated by (58) is compared with $U^D(r,\theta)$ calculated by the rigorous solution. The rigorous solutions of the potential $U(r,\theta)$ in the hard and soft wedges are given by [8], [9]

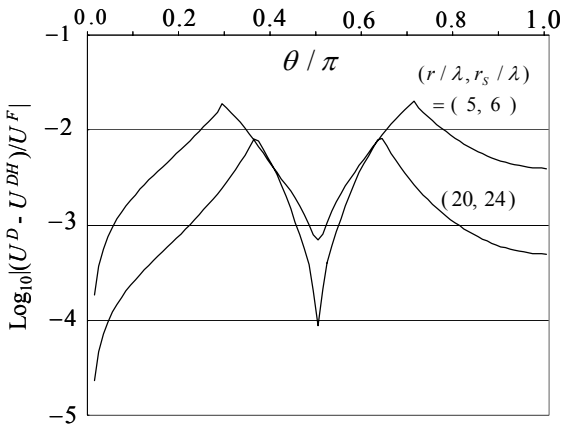

Figure 8 Error in the approximate solution in figures 6 and 7

$$
\begin{aligned}
&U(r,\theta \mid m=1)\\
&=-(\mathrm{j}\pi/4\Phi)\textstyle\sum_{p=0}^{\infty}\varepsilon_p \mathrm{J}_{pv}(kr)\mathrm{H}_{pv}^{(2)}(kr_S)\cos(pv(\theta+\Phi))\times\\
&\qquad\cos(pv(\theta_S+\Phi)),\\
&U(r,\theta \mid m=-1)\\
&=-(\mathrm{j}\pi/4\Phi)\textstyle\sum_{p=0}^{\infty}\varepsilon_p \mathrm{J}_{pv}(kr)\mathrm{H}_{pv}^{(2)}(kr_S)\sin(pv(\theta+\Phi))\\
&\qquad\times\sin(pv(\theta_S+\Phi)),
\end{aligned}
\tag{61}
$$

where $\nu=\pi/2\Phi$, J_{pv} and $H_{pv}^{(2)}$ stand for the Bessel function of real order and the second kind Hankel function of real order respectively, $\varepsilon_0 = 1$, $\varepsilon_p = 2$, $(p\neq 0)$, and $r < r_S$ is assumed. By subtracting the geometrical optics solution from the potential calculated by (61), the rigorous solution $U^D(r, \theta)$ is obtained.

The graphs of U^D and U^{DH} for $\Phi=\pi$, m=1 and θ_S=0.5 π are shown in figures 6 and 7. Since in this case U^D is anti-symmetric with respect to θ =0 [2], the graphs are shown only for $0.0< \theta/\pi < 1.0$. From (26), $\theta_{SB} = \pm 0.5\pi$. Thus the potential in these fugures changes discontinuously at $\theta = 0.5\pi$. Figure 6 corresponds to the graphs for r/λ=5.0 and r_S/λ =6.0 and figure 7 for r/λ=20.0 and r_S/λ=24.0. From (51), $\Omega=0.214\pi$ in figure 6 and 0.137π in figure 7. In the calculation of U^{DH}, the first term in the right side of (57) takes nonzero values for $|\theta - 0.5\pi| < \Omega$, that is, $0.286\pi < \theta < 0.714\pi$ in figure 6 and $0.363\pi < \theta < 0.637\pi$ in figure 7. The potentials in these graphs are normalized by that of the direct waves, that is, U^F and the real and imaginary parts of the normalized potential are shown in these figures. Consequently only the real part shows the jump of amplitude 1.0 at θ =0.5 π that corresponds to the angle for shadow boundary. Two Graphs in figure 7 are almost overlapping while in figure 6 the deviation of two graphs become evident around the switching angles θ=0.286 π and 0.714 π, especially in the imaginary part. The error in the approximate solution is evaluated in figure 8. As seen in this figure the error becomes largest at the switching angles and the high-frequency approximate solution is working properly in the vicinity of shadow boundary.

8. SUMMARY AND DISCUSSION

By applying the Huygens-Fresnel principle to the virtual space, a mathematical model for diffracted waves is constructed in terms of the elementary diffracted waves. By introducing the elementary diffracted waves, the physics of wedge diffraction and a new mechanism for generating diffracted waves are made clear. The elementary diffracted waves can be contained in the wave field in a pair and the pair of them is cancelled out each other except the wedge releases them from the cancellation. Thus simple and well-defined wave fields that contain no diffracted waves, such as free wave field and field in nondiffractive wedge, contain elementary diffracted waves in them and can be used as ideal wave fields for analyzing elementary diffracted waves. Consequently the high-frequency approximate solution of waves diffracted by the wedge for any observation angle can be deducted from our model. At the observation angle far from shadow boundaries, the deducted solution agrees to the conventional approximate solution derived from the rigorous solution literally. And our approximate solution works in the vicinity of shadow boundaries whereas in the conventional analysis it is not succeeded to derive the approximate solution that works in the vicinity of shadow boundaries [10]. The success of our model lies mainly in the simple structure of elementary diffracted waves around shadow boundary. Thus our top-down physical principle for diffraction is validated firmly by these results.

The virtual space is formulated by emitting wave rays from the observation point into all directions where the ray goes straight and is reflected at the boundary, and rearranging the potential on the ray as though it would go straight without reflection. Inversely the ray emitted from any point in the virtual space passes through the observation point. Thus if the secondary wavelet behaves like a particle in propagation and like a wave in addition, the application of the Huygens-Fresnel principle to the virtual plane corresponds to gathering all the secondary wavelets that attain the observation point to determine the potential at that point. The wave-particle duality that is popular in quantum physics, is also working at the core of diffraction process in classical physics and it gives the scheme to provide unique virtual space to each observation point. This simple and understandable principle deserves an underlying principle for wave propagation in a space that contains perfectly reflecting objects. This statement will be supported by the simplicity and effectiveness of the principle in analyzing various diffraction phenomena.

REFERENCES

1 Mitsuhiro Ueda, “A new representation of a scalar wave field diffracted by solid obstacles that satisfies both the wave equation and hard and soft boundary conditions”, J. Acoust. Soc. Am., 95, 2354-2362 (1994)

2 Mitsuhiro Ueda, “The physics of wedge diffraction: a model in terms of elementary diffracted waves”, J. Acoust. Soc. Am., 123, No.5, Pt.2 of 2, 3930 (May 2008)

3 M. Born and E. Wolf, Principles of optics (Pergamon Press, 1965) pp.375-382

4 Joseph B. Keller,” Geometrical theory of diffraction”, J. Opt. Soc. Amer., 52, 116-130 (1962)

5 A. F. Seybert and T. W. Wu, “Acoustic modeling: boundary element methods” in Encyclopedia of acoustics ed. Malcolm J. Crocker, (John Wiley & Sons, 1997), vol.1, pp.173-183

6 A.P.Prudnikov, Yu. A. Brychkov, O. I. Marichev, Integrals and series (Gordon and breach, 1986), vol.1,pp.646.

7 D.S.Jones, Acoustic and electeomagnitic waves (Clarendon Oxford 1986) pp.588

8 Ref.7, pp.586

9 Pyotr Ya. Ufimtsev, Fundamentals of the Physical Theory of Diffraction (John Wiley & Sons, 2007) pp.38

10 Ref.9, pp.47-55